

## $\pi^+p$ , $K^+p$ , and $pp$ topological cross sections and inclusive interactions at 100 GeV using a hybrid bubble-chamber-spark-chamber system and a tagged beam\*

W. M. Morse, V. E. Barnes, D. D. Carmony, R. S. Christian, A. F. Garfinkel, and L. K. Rangan

*Physics Department, Purdue University, West Lafayette, Indiana 47907*

A. R. Erwin, E. H. Harvey, R. J. Loveless, and M. A. Thompson

*Physics Department, University of Wisconsin, Madison, Wisconsin 53706*

(Received 21 May 1976)

$\pi^+p$ ,  $K^+p$ , and  $pp$  interactions at 100 GeV are studied using the Fermilab hybrid 30-inch bubble chamber with associated downstream multiparticle spectrometer and an unseparated tagged positive beam. Topological cross sections and charged-particle-multiplicity moments are presented and good agreement is found with Koba-Nielsen-Olesen scaling. The charged-multiplicity second moment,  $f_2^{cc}$ , and the second moment of produced  $(+ -)$  pairs,  $f_2^{-}$ , are presented both with and without the diffractive-dissociation events, and are discussed in terms of the two-component model invoked to explain  $pp$  multiplicity distributions above 100 GeV. Single-particle inclusive distributions are presented and studied in terms of the Regge-Mueller forms of approach to scaling at asymptotic energies. Pomeron factorization is found to hold in the target-proton-associated backward center-of-mass hemisphere for inclusive particle production by incident  $\pi^+$ ,  $K^+$ , and protons.

### I. INTRODUCTION

$\pi^+p$  inclusive interactions have been studied extensively at beam energies below 30 GeV. This is the first experiment to study  $\pi^+p$  inclusive interactions at Fermi National Accelerator Laboratory (Fermilab) energies with good momentum resolution over the entire kinematically allowed range. The apparatus consists of the Fermilab 30-in. hydrogen bubble chamber, upstream proportional wire chambers, and downstream optical spark chambers. The 100-GeV/c tagged beam contains 50% protons, 46%  $\pi^+$ , 2.7%  $\mu^+$ , and 1.5%  $K^+$  at the bubble chamber. The beam, apparatus, and reconstruction programs have been discussed elsewhere.<sup>1,2</sup>

Shown in Fig. 1(a) is the momentum distribution determined in the bubble chamber alone for positive tracks from a large sample of two-, four-, and six-prong events.<sup>3</sup> The HOOKUP-determined momentum of the same tracks is shown in Fig. 1(b), where full use has been made of both spark-chamber and bubble-chamber measurement of track coordinates.<sup>4</sup> The HOOKUP momentum distribution shows a prominent peak at 100 GeV/c due to elastic and quasielastic scattering. The resolution of the bubble-chamber measurement alone is too poor to see this peak.

The  $\pi^+p$ ,  $K^+p$ , and  $pp$  total cross sections determined by this experiment<sup>1,2</sup> are in good agreement with those measured by the Fermilab-BNL-Rockefeller collaboration using electronic-counter techniques.<sup>5</sup> Therefore we have normalized all of our

cross sections such that our total cross sections are equal to those of Ref. 5. This yields a microbarn equivalent for  $\pi^+p$  ( $pp$ ) events of 5.3 (5.0)  $\mu\text{b}/\text{event}$  for two-, four-, and six-prong events and 7.0 (6.7)  $\mu\text{b}/\text{event}$  for the higher-multiplicity events which were measured for a subset of our total exposure.

Elastic events ( $\pi^+p \rightarrow \pi^+p$  and  $pp \rightarrow pp$ ) have been identified with the kinematic fitting program SQUAW and removed from the sample of events to be discussed. The  $\pi^+p$ ,  $K^+p$ , and  $pp$  elastic cross

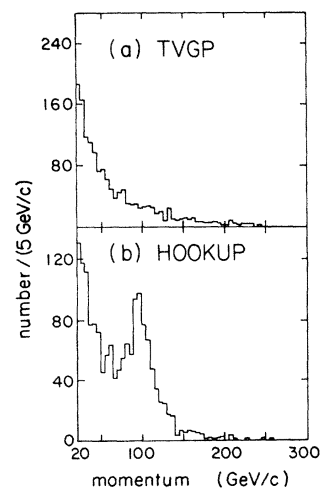


FIG. 1. TVGP bare bubble-chamber and HOOKUP-measured momentum of positive tracks from two-, four-, and six-prong events.

sections measured in this experiment<sup>6</sup> are in good agreement with recent Fermilab counter measurements.<sup>7</sup>

Protons with ionization greater than 1.5 times minimum ionization (lab momentum less than 1.3 GeV/c) were identified during the scanning process. The slow-proton inclusive distributions have been discussed elsewhere.<sup>1,6</sup> Such identified protons are not included in the inclusive  $\pi^+$  sample to be discussed here.

## II. TOPOLOGICAL CROSS SECTIONS

The inelastic topological cross sections and moments for  $\pi^+p$ ,  $K^+p$ , and  $pp$  scattering are shown in Table I. The average charged multiplicity  $\langle n \rangle$ , dispersion squared  $D^2$ , and charged-charged moment  $f_2^{cc}$  are defined by

$$\langle n \rangle = \frac{\sum_n n \sigma_n}{\sum_n \sigma_n}, \quad (1)$$

$$D^2 = \langle n^2 \rangle - \langle n \rangle^2, \quad (2)$$

$$f_2^{cc} = D^2 - \langle n \rangle, \quad (3)$$

where  $\sigma_n$  is the topological cross section for events of charged multiplicity equal to  $n$ . The cross sections are corrected for scanning efficiencies and loss of small- $l$  two-prong events. The small number of odd-prong events (ten out of seven thousand) are added to the next higher multiplicity. All the odd-prong events have one more positive track than negative track and are confined to the low

multiplicities. Thus these events are consistent with being very-small- $l$  scatterings where the recoil proton is too short to observe. None of these events is consistent with having a  $\delta$  ray misidentified as a negative hadron.

The topological cross sections have been corrected for undetected  $e^+e^-$  Dalitz pairs from  $\pi^0$ 's. Assuming that the average number of  $\pi^0$ 's equals the average number of  $\pi^-$ 's, and using the observed  $K^0$ 's to correct for  $K^-$ , we expect one event in 41 to have a Dalitz pair, that is, 175 expected Dalitz pairs. We observed 87 Dalitz pairs in the  $\pi^+p$  and  $pp$  event scan. The 88 presumed undetected Dalitz pairs were assumed to have the same multiplicity distribution as the detected Dalitz pairs.

Also shown in Table I are the 100-GeV/c  $\pi^+p$  and  $pp$  ( $pp$ ) topological cross sections of Ref. 8 (9). The results of Ref. 8 (9) are based on about one-half (90%) as many events as are in our data sample. The total cross sections of Refs. 8 and 9 were not normalized to those of Ref. 5, but were experimentally determined. Apart from normalization differences, the data are in reasonable agreement.

Koba, Nielsen, and Olesen<sup>10</sup> (KNO) have shown that if the structure function  $(2E/\pi\sqrt{s})(d^2\sigma/dx dp_T^2)$  scales at asymptotic energies, the energy dependence of the partial cross sections is contained in the variable  $n/\langle n \rangle$ . The KNO scaling prediction is

$$\frac{\sigma_n(s)}{\sigma_{\text{inel}}(s)} = \frac{1}{\langle n \rangle} \psi\left(\frac{n}{\langle n \rangle}\right) + O\left(\frac{1}{\langle n \rangle^2}\right), \quad (4)$$

TABLE I. Inelastic topological cross sections.

Prong No.	$pp$ (100 GeV/c)				$\pi^+p$ (100 GeV/c)			$K^+p$ (100 GeV/c)	
	No. observed	$\sigma$ (mb)	Ref. 8	Ref. 9	No. observed	$\sigma$ (mb)	Ref. 8	No. observed	$\sigma$ (mb)
2	586	4.91±0.33	4.6±0.7	4.5±0.4	272	2.38±0.20	2.8±0.7		2.33±0.85
3	4				4				
4	1029	7.31±0.26	7.54±0.31	7.9±0.3	619	4.65±0.20	4.12±0.25	46	3.50±0.49
5	1				1				
6	990	7.01±0.25	7.73±0.31	7.5±0.3	662	4.82±0.21	5.54±0.29	42	3.11±0.47
8	800	5.60±0.22	5.58±0.26	5.8±0.2	489	3.63±0.17	4.42±0.25	47	3.79±0.51
10	533	3.73±0.17	3.90±0.22	3.7±0.2	362	2.64±0.15	2.77±0.20	24	1.83±0.38
12	244	1.69±0.11	2.01±0.16	1.6±0.1	176	1.25±0.10	1.50±0.15	13	1.00±0.29
14	116	0.81±0.08	0.78±0.10	0.62±0.07	66	0.49±0.06	0.55±0.09	6	0.48±0.20
16	31	0.21±0.04	0.31±0.06	0.21±0.04	21	0.13±0.03	0.23±0.06		
18	10	0.07±0.02	0.06±0.04	0.05±0.02	6	0.04±0.02	0.09±0.04	2	0.18±0.13
20	1	0.01±0.01	0.04±0.03	0.016±0.011	2	0.02±0.01	0.03±0.02		
Total	4345	31.4±0.2	32.5±0.9	31.9±0.7	2680	20.0±0.2	22.0±0.9		16.2±0.2
$\langle n \rangle$		6.37±0.06	6.49±0.10	6.32±0.07		6.62±0.07	6.80±0.14		6.65±0.31
$D^2$		10.6±0.3		9.80±0.25		10.2±0.3			11.2±1.3
$f_2^{cc}$		4.2±0.3		3.45±0.25		3.6±0.3			4.5±1.3
$f_2^{-}$		0.46±0.08		0.28±0.07		0.25±0.08			0.47±0.36

where  $\sigma_{\text{inel}} \equiv \sigma_{\text{tot}} - \sigma_{\text{el}}$ . Our  $\pi^+p$ ,  $K^+p$ , and  $pp$  topological cross sections are shown in Fig. 2. The solid line is a fit to the  $pp$  data at momenta of 50, 69, 102, 205, and 303 GeV/c,<sup>11</sup> in good agreement with our  $pp$  data. Furthermore, our  $\pi^+p$  and  $K^+p$  data are well described by the curve.

Our 100-GeV/c  $pp$  average charged multiplicity,  $6.37 \pm 0.06$ , is consistent with world data from 50 to 2000 GeV, which are well fitted by any of the functional forms<sup>12</sup>

$$\langle n_c \rangle = -2.9 \pm 0.3 + (1.79 \pm 0.05) \ln(s), \quad (5)$$

$$\langle n_c \rangle = A + B \ln(s) + Cs^{-1/2}, \quad (6)$$

$$\langle n_c \rangle = A + B \ln(s) + C \ln^2(s). \quad (7)$$

The 100-GeV/c  $\pi^+p$  average multiplicity is several standard deviations greater than the 100-GeV/c  $pp$  average multiplicity, the difference for our data being  $+0.26 \pm 0.09$ . This can be explained qualitatively by a quark picture where the proton beam is made up of three quarks and the beam pion is made up of two quarks. If particles are produced predominantly by the collision of a single quark from the beam with a single quark from the target, then  $\sqrt{s_{qq}}$ , the total energy in the quark-quark center of mass, should control the mean multiplicity of particles produced. If the valence quarks carry most of the momentum in the hadron, one can easily show that  $s_{qq} = s/6$  for  $\pi^+p$  scattering and  $s_{qq} = s/9$  for  $pp$  scattering. Hence, if  $\langle n \rangle$  varies as  $\ln(s)$ , it will also vary as  $\ln(s_{qq})$  and we expect  $\langle n(\pi^+p) \rangle - \langle n(pp) \rangle = 1.8[\ln(\frac{1}{6}) - \ln(\frac{1}{9})] = 0.7$ , independent of  $s$ . This is larger than we observe. The inclusion of "sea" quarks and/or "gluons" could make this model consistent with our data.

The 100-GeV/c  $K^+p$  average multiplicity is inter-

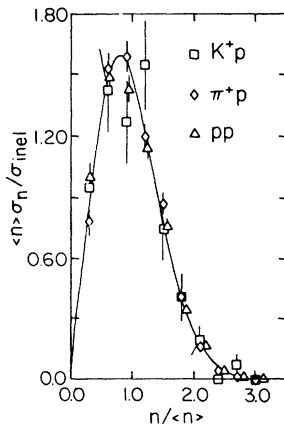


FIG. 2.  $K^+p$ ,  $\pi^+p$ , and  $pp$  topological cross sections at 100 GeV/c:  $\langle n \rangle \sigma_n / \sigma_{\text{inel}}$  vs  $n / \langle n \rangle$ . The curve is a fit to  $pp$  topological cross sections at momenta of 50, 69, 102, 205, and 303 GeV/c, Ref. 11.

mediate between the  $\pi^+p$  and  $pp$  multiplicities and consistent with either, within the statistical uncertainty.

The second moments of the charged-particle multiplicity distributions,  $f_2^{cc} = D^2 - \langle n \rangle$ , rise several units from  $f_2^{cc} \approx 0$  at 30 GeV/c.<sup>20</sup> The Poisson distribution predicted by a simple multiperipheral model has  $\langle n \rangle = D^2$  and thus  $f_2^{cc} = 0$ .<sup>13</sup> At 100 GeV/c the values of  $f_2^{cc}$  for  $\pi^+p$ ,  $K^+p$ , and  $pp$  are all consistent with each other and reflect a significantly wider distribution than a Poisson distribution. On the other hand, the second moments of produced (+ -) pairs,  $f_2^{--}$ , which are also presented in Table I, are small but are several standard deviations positive, consistent with nearly Poisson distributions in  $pp$ ,  $\pi^+p$ , and  $K^+p$  interactions at 100 GeV. Several authors have attributed an increase in  $f_2^{--}$  at energies above 100 GeV to the presence of two components: diffractive and multiparticle production.<sup>14</sup>

We shall now compare our data to a two-component hypothesis. Shown in Table II are the two-, four-, and six-prong topological cross sections with single-diffractive excitation events removed for  $\pi^+p$  and  $pp$  collisions.<sup>15</sup> We see no evidence for a diffractive component in the higher multiplicities at 100 GeV.<sup>5</sup> The average multiplicity is  $3.10 \pm 0.14$  for  $\pi^+p$  diffractive excitation events ( $\pi^+p - \pi^+p^*$  and  $\pi^+p - \pi^+p^*$ ) and  $2.80 \pm 0.09$  for  $pp$  diffractive excitation events ( $pp - p^*p$  and  $pp - pp^*$ )—less than one-half the nondiffractive average charged multiplicity.<sup>5</sup> The inelastic two-prong cross sections are dominated by diffractive excitation which explains their very slow decrease with energy. The moments  $f_2^{cc}$  and  $f_2^{--}$  for this nondiffractive part of the  $\pi^+p$  and  $pp$  inclusive samples are given in Table II. The single-charged-particle production distributions are similar in  $\pi^+p$  and  $pp$  interactions and remain substantially wider than Poisson distributions, while the (+ -) pair distributions from  $\pi^+p$  and  $pp$  interactions are slightly

TABLE II. Two-, four-, and six-prong nondiffractive cross sections and nondiffractive multiplicity distribution moments for all multiplicities at 100 GeV.

Prong No.	$\pi^+p$ $\sigma$ (mb)	$pp$ $\sigma$ (mb)
2	$0.52 \pm 0.17$	$1.15 \pm 0.20$
4	$3.14 \pm 0.15$	$5.27 \pm 0.19$
6	$4.61 \pm 0.21$	$6.79 \pm 0.25$
$\langle n \rangle$	$7.41 \pm 0.08$	$7.23 \pm 0.06$
$D^2$	$8.9 \pm 0.4$	$9.1 \pm 0.3$
$f_2^{cc}$	$1.5 \pm 0.4$	$1.9 \pm 0.3$
$f_2^{--}$	$-0.48 \pm 0.10$	$-0.33 \pm 0.08$

narrower than Poisson distributions, as indicated by the values of  $f_2^-$  which are small but several standard deviations negative.

### III. RAPIDITY AND REGGE-MUELLER THEORY

We shall use the rapidity variable,  $y$ , in discussing the inclusive reactions

$$A + B \rightarrow C + X. \quad (8)$$

The variable  $y$  denotes the rapidity of produced particles while  $Y$  denotes the laboratory rapidity of the incoming particle. Here  $X$  signifies anything physically allowed to complete the final state. We define

$$y \equiv \sinh^{-1} \left( \frac{p_{\parallel}}{\mu} \right), \quad (9)$$

where  $p_{\parallel}$  is the longitudinal component of the momentum and  $\mu$  is the "transverse mass," with  $\mu^2 = m^2 + P_T^2$ , so that  $(E^2 = p_{\parallel}^2 + \mu^2)$ . The longitudinal Lorentz transformation specified by a boost  $\xi$  is given by

$$\begin{pmatrix} E \\ p_{\parallel} \end{pmatrix}' = \begin{pmatrix} \cosh \xi & -\sinh \xi \\ -\sinh \xi & \cosh \xi \end{pmatrix} \begin{pmatrix} E \\ p_{\parallel} \end{pmatrix} \quad \text{and} \quad y' = y - \xi. \quad (10)$$

The laboratory beam rapidity  $Y \simeq \ln(s/m_A m_B)$  at high energies. The transformation from the lab to the center-of-mass system is given by

$$y^* = y_L - \sinh^{-1} \frac{p_B^*}{m_B}, \quad (11)$$

where starred quantities are in the center-of-mass system.

The single-particle Lorentz-invariant phase space is  $d^3p/E$ . Thus in terms of the variables  $p_{\parallel}$ ,  $p_T^2$ ,  $y$ , and Feynman  $x \equiv 2p_{\parallel}^*/\sqrt{s}$ , the structure functions for the reaction (8) are

$$\begin{aligned} f(\vec{p}, s) &= \frac{Ed^3\sigma}{d^3p} = \frac{E}{\pi} \frac{d^2\sigma}{dp_{\parallel} dp_T^2} = \frac{2E}{\pi\sqrt{s}} \frac{d^2\sigma}{dx dp_T^2} \\ &= \frac{1}{\pi} \frac{d^2\sigma}{dy dp_T^2}. \end{aligned} \quad (12)$$

Whereas the optical theorem relates the total cross section to the imaginary part of the two-body scattering amplitude, Regge-Mueller theory<sup>13</sup> uses a generalized optical theorem to relate the inclusive cross section for the process  $A + B \rightarrow C + X$  to the imaginary part of the scattering amplitude for the three-body process  $A\bar{C}B \rightarrow A\bar{C}B$ :

$$\frac{d^2\sigma}{dy dp_T^2} (A + B \rightarrow C + X) \sim \frac{\text{Im} \mathcal{Q}(A\bar{C}B \rightarrow A\bar{C}B)}{s} \Big|_{\text{forward}} \quad (13)$$

Consider the case when particle  $C$  is in the central region  $Y_B^* \ll y_C^* \ll Y_A^*$ . Then  $d^2\sigma/dy dp_T^2$  is related to the diagram shown in Fig. 3(a). According to Regge theory

$$\mathcal{Q}|_{\text{forward}} \sim \beta_A(-t)^{\alpha_i(0)} \beta_C(-u)^{\alpha_j(0)} \beta_B. \quad (14)$$

When the quantum numbers of  $A\bar{C}B$  are exotic, the exchange trajectories will be dominated by the Pomeron. Then

$$\frac{d^2\sigma}{dy dp_T^2} \sim \beta_C(p_T^2) s^{\alpha(0)-1} \beta_A \beta_B. \quad (15)$$

If we divide by  $\sigma_T(AB) = \beta_A \beta_B s^{\alpha(0)-1}$  we find  $(1/\sigma_T)(d^2\sigma/dy dp_T^2) \sim \beta_C(p_T^2)$ . This is a remarkable result. It predicts that in the central region  $\mathcal{R}_{AB}^C \equiv (1/\sigma_T)(d^2\sigma/dy dp_T^2)$  is independent of  $s$ ,  $y$ , and the quantum numbers of the beam and target. Including the Pomeron-Regge and Regge-Regge exchanges adds terms that have  $s^{-1/4}$  and  $s^{-1/2}$  dependences.

When particle  $C$  is in the fragmentation region ( $Y_A^* > y_C^* \gg Y_B^*$ ), Fig. 3(b) applies. Then

$$\mathcal{Q}|_{\text{forward}} \sim \beta_{AC}(p_T^2, y)(-u)^{\alpha_j(0)} \beta_B \quad (16)$$

and

$$\mathcal{R}_{AB}^C \sim \frac{\beta_{AC}(p_T^2, y)}{\beta_A}, \quad (17)$$

if the exchange is dominated by the Pomeron. Note that this distribution is independent of particle  $B$  and of  $s$ . Inclusion of lower-lying trajectories adds terms with  $s^{-1/2}$  dependence. We will compare our data with the prediction of factorization implied by Eq. (17) (for example,  $\mathcal{R}_{pp}^{\pi^+} = \mathcal{R}_{\pi^+p}$  when  $y_{\pi^+}^* \ll Y_{\text{beam}}^*$ ).

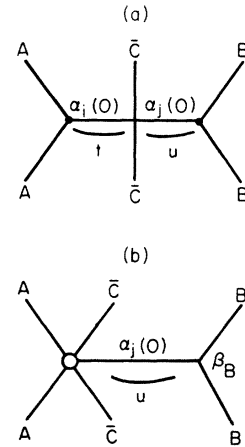


FIG. 3. Regge-Mueller diagrams for (a) central and (b) fragmentation kinematic regions.

## IV. TESTS OF FACTORIZATION

Shown in Figs. 4, 5, and 6 are the structure functions

$$\rho(y^*) \equiv \int \mathcal{R}(y^*, p_T^2) dp_T^2 = \int \frac{dp_T^2}{\sigma_T} \frac{d\sigma}{dy^* dp_T^2} \quad (18)$$

for  $A + p \rightarrow C^\pm + X$ , where  $A = \pi^+$ ,  $p$ , or  $K^+$ .  $C^-$  is largely  $\pi^-$  with less than 10% contamination by  $\bar{p}$  and  $K^-$ . Forward  $C^+$  from  $pp$  ( $K^+p$ ) interactions will be significantly contaminated with  $p$  ( $K^+$ ). Moreover, there is a problem with proton identification in the backward hemisphere for all  $A$ . Protons with lab momentum less than 1.3 GeV/c (1.5 times minimum ionization) are identified and removed. Such protons with  $p_{||} < 1$  GeV/c correspond to  $y^* < -2.1$ . Protons with  $p > 1.3$  GeV/c are assumed to be pions and, since the rapidity is an explicit function of mass, appear with an incorrect rapidity. For Feynman  $x \leq -0.5$  we have a fairly clean sample of  $\pi^+$ , as we do for  $\pi^+p \rightarrow \pi^+$  in the forward hemisphere. We shall refer to  $C^\pm$  as  $\pi^\pm$  from now on, with contamination as described above. Elastic events have been removed in all cases.

The  $pp \rightarrow \pi^\pm$  structure functions are shown in Fig. 5. The  $pp$  distributions are expected to be symmetric about  $y^* = 0$ . The  $pp \rightarrow \pi^-$  distribution is symmetric, and the  $pp \rightarrow \pi^+$  distribution in the central region ( $Y_A^* \gg y^* \gg Y_B^*$ ) is also consistent with symmetry. The excess at  $y > 2$  is caused by unidentified fast protons, whereas slow protons in the backward hemisphere have been identified by ionization and removed, as described above.

The  $\pi^+p \rightarrow \pi^\pm$  structure functions of Fig. 4 do not peak at  $y^* = 0$ , but rather at positive  $y^*$ . The quark

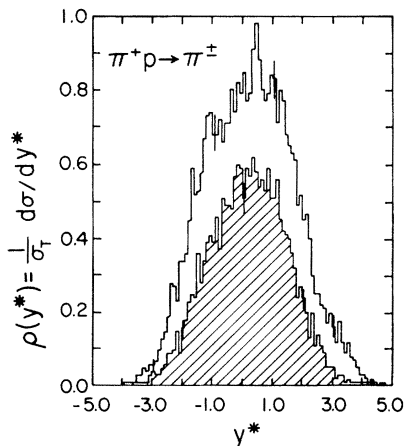


FIG. 4.  $(1/\sigma_T)d\sigma/dy^*$  structure functions for the reactions  $\pi^+p \rightarrow \pi^+$  and  $\pi^+p \rightarrow \pi^-$  (shaded).

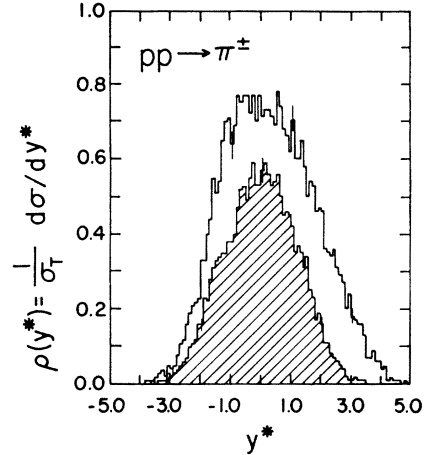


FIG. 5.  $(1/\sigma_T)d\sigma/dy^*$  structure functions for the reactions  $pp \rightarrow \pi^+$  and  $pp \rightarrow \pi^-$  (shaded).

picture predicts that they will be centered about  $y' = 0$ , where  $y'$  is calculated in the quark-quark center of mass. The boost parameter to go to this system is

$$\xi = \frac{1}{2} \ln\left(\frac{2}{3}\right) = -0.20. \quad (19)$$

Our  $\pi^+p \rightarrow \pi^\pm$  distributions are consistent with peaking at  $y^* = +0.20$ , as predicted.

The  $K^+p \rightarrow \pi^\pm$  structure functions are shown in Fig. 6. The tendency for the  $\pi^-$  distribution to peak at a negative value of  $y^*$  is discussed elsewhere<sup>16</sup> in terms of a valence-quark momentum picture.

It can be seen that 100 GeV/c is not yet an asymptotic energy in the Regge-Mueller sense. The  $A p \rightarrow \pi^+$  structure function is greater than the  $A p \rightarrow \pi^-$  structure function in the central region ( $A$  is  $\pi^+$ ,  $K^+$ , or  $p$ ). Thus the central region "remembers" that the beam (target) has positive charge. Also there is little evidence for a central plateau in rapidity.

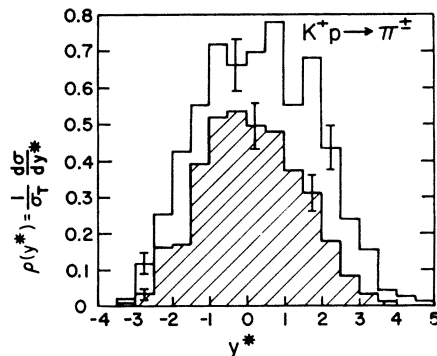


FIG. 6.  $(1/\sigma_T)d\sigma/dy^*$  structure functions for the reactions  $K^+p \rightarrow \pi^+$  and  $K^+p \rightarrow \pi^-$  (shaded).

The ratios

$$R_{\pi^-}(y^*) \equiv \frac{\rho_{\pi^+p}^{\pi^-}(y^*)}{\rho_{pp}^{\pi^-}(y^*)} \quad \text{and} \quad R_{\pi^+}(y^*) \equiv \frac{\rho_{\pi^+p}^{\pi^+}(y^*)}{\rho_{pp}^{\pi^+}(y^*)} \quad (20)$$

are shown in Figs. 7(a) and 7(b). Our data are in good agreement with those of Ref. 17. Regge-Mueller theory predicts these ratios to be 1.0 in the backward hemisphere when a factorizable Pomeron dominates the diagram shown in Fig. 3(b). In the backward hemisphere  $R_{\pi^-}(y^*)$  is consistent with unity while  $R_{\pi^+}(y^*)$  is greater than unity. Thus factorization is satisfied at 100 GeV/c when the  $A\bar{C}B$  quantum numbers are exotic, but not when the  $A\bar{C}B$  quantum numbers are not exotic, as predicted by the generalized optical theorem.

$R_{\pi^-}$  is significantly greater than unity only in the forward part of the forward hemisphere. Thus the excess of  $\langle n^-(\pi^+p) \rangle$  over  $\langle n^-(pp) \rangle$  comes entirely from this forward region. Thus  $\pi^+$  beam fragmentation appears to produce more fast  $\pi^-$  than does proton beam fragmentation. The excess of  $\langle n^+(\pi^+p) \rangle$  over  $\langle n^+(pp) \rangle$  occurs in both the forward and backward hemispheres.

The ratios

$$R_{K^-}(y^*) = \frac{\rho_{K^+p}^{K^-}}{\rho_{pp}^{K^-}} \quad \text{and} \quad R_{K^+}(y^*) = \frac{\rho_{K^+p}^{K^+}}{\rho_{pp}^{K^+}} \quad (21)$$

are shown in Fig. 8. Since the quantum numbers of  $A\bar{C}B$  are exotic for all four inclusive reactions involved in Eq. (20), Regge-Mueller theory predicts  $R_{K^+}$  and  $R_{K^-}$  to be unity in the backward hemisphere of the center of mass. Both  $R_{K^+}$  and  $R_{K^-}$  are consistent with unity within statistics for  $y^* < 0$ . As with the  $\pi^+p$  data,  $R_{K^-}$  is greater than unity for  $y^* > 1.0$ .

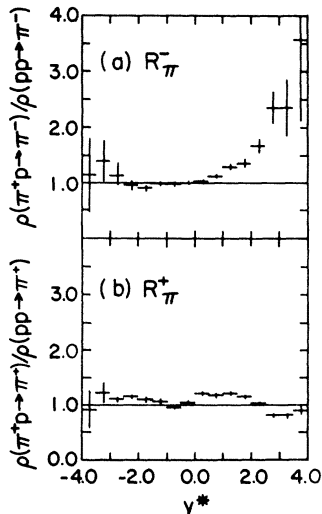


FIG. 7.  $R_{\pi^-}$  and  $R_{\pi^+}$  as function of  $y^*$  [see Eq. (20)].

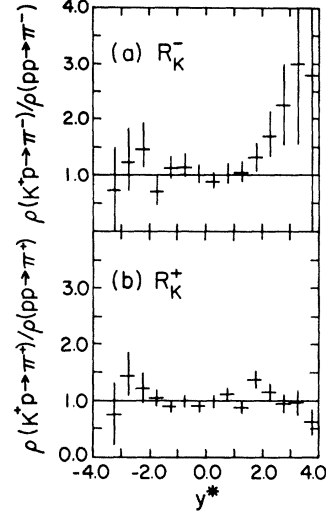


FIG. 8.  $R_{K^-}$  and  $R_{K^+}$  as function of  $y^*$  [see Eq. (21)].

## V. TESTS OF SCALING

Feynman and Benecke, Chou, Yang, and Yen first predicted that at asymptotic energies, the structure function for the inclusive reaction (8) would become independent of energy.<sup>18,19</sup> This is called the hypothesis of scaling. As seen above, Regge-Mueller theory predicts the structure function will have the form  $a + bs^{-1/4}$  in the central region, and  $a + bs^{-1/2}$  in the fragmentation regions. Furthermore, Regge-Mueller theory predicts early scaling (small- $b$  parameter) when the quantum numbers of  $A\bar{C}B$  are exotic.

Plotted in Fig. 9 is the structure function

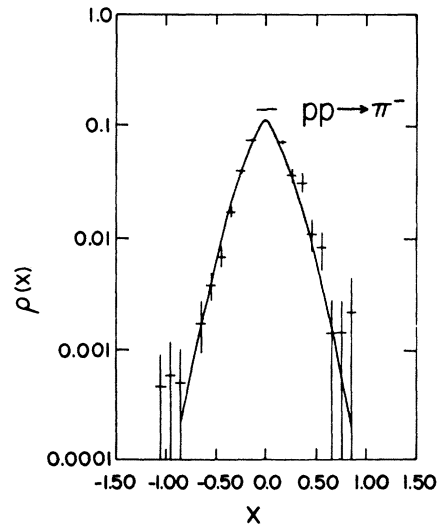


FIG. 9.  $\rho(x)$  structure function [see Eq. (22)] for reaction  $pp \rightarrow \pi^-$ . The curve is a symmetric fit to data from 28.5 GeV/c, Ref. 20.

$$\rho(x) = \int \frac{2E^*}{\pi\sigma_T\sqrt{s}} \frac{d^2\sigma}{dp_T^2 dx} dp_T^2 \quad (22)$$

for the reaction  $pp \rightarrow \pi^- + X$  at 100 GeV. The curve is a symmetrical fit representing the data from 28.5 GeV/c.<sup>20</sup> There has been a 50% increase in the value of the  $pp \rightarrow \pi^-$  structure function evaluated at  $x=0$  from that found at 28.5 GeV/c. However, we find scaling within 10% for  $|x| > 0.2$ . When fitted to the function  $\rho(x) = Ae^{B|x|}$ ,  $A = 0.196 \pm 0.004$  and  $B = -6.73 \pm 0.18$ .

We have not invoked the symmetry of the  $pp$  interaction in our  $\rho(x)$  distribution and in order to increase our resolution, we have used for  $x > 0.2$  only those tracks which "hook up" to the downstream system, weighting these fast tracks according to the overall hook-up acceptance. If the hook-up corrections are properly done, we expect symmetry about  $x=0$  because of the symmetry of the initial state. Taking into account the broader momentum resolution as  $x \rightarrow +1$ , our distribution is consistent with being symmetric about  $x=0$  as it should be. This gives us further confidence in our forward inclusive  $\pi^+p$  distributions which are available for the first time at Fermilab energies in this experiment.

Plotted in Figs. 10(a) and 10(b) are the structure functions  $\rho(x)$  for the reactions  $\pi^+p \rightarrow \pi^+$  at 100 GeV with elastic events removed. Only tracks which hook up are used for  $x > 0.2$  and tracks that do not hook up are corrected for. The circles represent data from Ref. 21 at 16 GeV/c. The  $\pi^+p \rightarrow \pi^-$  inclusive distribution shows an increase over the 16-GeV/c values in the central region for  $-0.3 < x < 0.1$ , but approximate scaling is seen in the

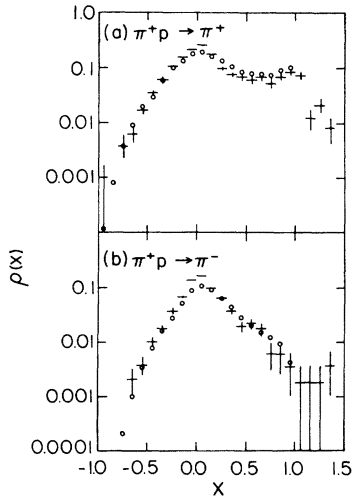


FIG. 10.  $\rho(x)$  structure functions [see Eq. (22)] for reactions  $\pi^+p \rightarrow \pi^+$  and  $\pi^+p \rightarrow \pi^-$ . Circles represent data from 16 GeV/c, Ref. 21.

beam- and target-fragmentation regions for  $x < -0.3$  and  $0.2 < x$ . Beaupré *et al.*<sup>21</sup> examining data at 8 and 16 GeV/c found that the reaction  $\pi^+p \rightarrow \pi^-$  scales for  $x < -0.3$  and  $0.3 < x < 0.7$ . Scaling within 10% is seen for the  $\pi^+p \rightarrow \pi^+$  inclusive distribution for  $x < -0.2$ , but the structure function for  $0.2 < x < 0.8$  is smaller at 100 GeV than at 16 GeV. Beaupré *et al.* found that the  $\pi^+p \rightarrow \pi^+$  structure function for  $0.2 < x < 0.8$ , and also for  $x < -0.2$ , decreases with increasing beam energy between 8 and 16 GeV.

When  $\rho_{\pi^+p}^{\pi^+}$  is fitted to the function  $ae^{b|x|}$ , we find  $a = 0.207 \pm 0.005$  and  $b = -4.65 \pm 0.18$  for the forward hemisphere, and  $a = 0.193 \pm 0.005$  and  $b = -6.83 \pm 0.23$  for the backward hemisphere of the center of mass. The fit to  $\rho_{\pi^+p}^{\pi^-}$  for the backward hemisphere of the center of mass is in excellent agreement with the fit of the  $pp \rightarrow \pi^-$  structure function  $\rho_{pp}^{\pi^-}$  ( $a = 0.196 \pm 0.004$  and  $b = -6.73 \pm 0.18$ ).

We also note that there are more  $\pi^-$ 's in the forward center-of-mass hemisphere than in the backward hemisphere for  $\pi^+p$  interactions ( $b_{\text{forward}} - b_{\text{backward}} = 2.18 \pm 0.29$ ), reflecting the difference between the pion beam and the proton target.

This excess of pions in the pion-beam hemisphere can be attributed in part to  $G$ -parity constraints which require pion dissociation into at least three pions while nucleons can dissociate into  $N\pi$ . Additionally, the valence-quark picture predicts that the produced pions in  $\pi p$  interactions will be shifted forward in rapidity.

All structure functions examined have shown an increase over lower energy data for  $x \approx 0$ . Ferbel<sup>22</sup> suggests plotting the inclusive distribution at  $y^* = 0$  vs  $p_T^{-1/4}$ , which is approximately proportional to  $s^{-1/4}$ . Regge-Mueller theory predicts that the structure function  $\mathcal{R}(y^*, p_T^2)$  will scale at asymptotic energies and will approach the scaling limit with a term varying as  $s^{-1/4}$ . Erwin *et al.*<sup>17</sup> show  $\rho(y^* = 0)$  for the reactions  $\pi^+p \rightarrow \pi^+$ ,  $\pi^+p \rightarrow \pi^-$ ,  $pp \rightarrow \pi^+$ , and  $pp \rightarrow \pi^-$  as a function of  $p_T^{-1/4}$ . The data lie on straight lines which intersect at a universal point  $\rho(y^* = 0) \approx 0.75$ . Our values of  $\rho(y^* = 0)$  are shown in Table III. The values corrected for  $K^{\pm}$  and proton contamination are also shown.<sup>23</sup> These corrected values are in good agreement with the data of Erwin *et al.*<sup>17</sup> New results at higher energies,<sup>24</sup> however, are not consistent with the extrapolation of lower-energy data to the point  $\rho(y^* = 0) \approx 0.75$ . It is interesting that all the data approach the possible scaling limit from below, whereas the simpler Regge-Mueller-type models predict an approach from above.

Shown in Fig. 11 is the structure function  $\rho(x)$  evaluated at  $x = -0.5$  vs  $s^{-1/2}$ .<sup>20,21,25-27</sup> We have used the 100-GeV/c values for the total cross sections. Protons have been identified by ionization

TABLE III.  $(1/\sigma_T)d\sigma/dy^*|_{y^*=0}$  at 100 GeV.

	$\pi^+p \rightarrow \pi^+$	$\pi^+p \rightarrow \pi^-$	$pp \rightarrow \pi^+$	$pp \rightarrow \pi^-$
Uncorrected	$0.809 \pm 0.018$	$0.565 \pm 0.015$	$0.729 \pm 0.013$	$0.556 \pm 0.011$
Corrected for protons and $K^\pm$ (see Ref. 23)	$0.716 \pm 0.021$	$0.512 \pm 0.016$	$0.604 \pm 0.017$	$0.521 \pm 0.012$

in this kinematic region. Within the experimental uncertainties all structure functions are consistent with scaling as  $s^{-1/2}$  as predicted by Regge-Mueller theory for the fragmentation regions.<sup>28</sup> Furthermore, the reaction  $Ap \rightarrow \pi^-$  in the target-fragmentation region is consistent with being independent of the beam quantum numbers at asymptotic energies:

$$\lim_{s \rightarrow \infty} \rho_{pp}^{\pi^-}(x = -0.5) = \rho_{\pi^-p}^{\pi^-}(x = -0.5) = \rho_{\pi^+p}^{\pi^-}(x = -0.5),$$

while the asymptotic  $\pi^+p \rightarrow \pi^+$  value is approximately three times larger.

The  $\rho(x)$  structure function evaluated at  $x = +0.5$  vs  $s^{-1/2}$  is shown in Fig. 12. As with Fig. 11 the data are consistent with scaling as  $s^{-1/2}$  and  $\rho_{\pi^+p}^{\pi^+}(x = 0.5)$  is about three times greater than  $\rho_{\pi^+p}^{\pi^-}(x = 0.5)$  at asymptotic energy. Although the data are consistent with scaling in  $x$  at the rate predicted by Regge-Mueller theory, the exact energy dependence of scaling and the asymptotic scaling form must await higher statistics and higher-energy

experiments.<sup>28</sup>

The value of  $\rho_{pp}^{\pi^+}(x = -0.5)$  is plotted for our 100-GeV data in Fig. 11, where it is close to the value of  $\rho_{\pi^+p}^{\pi^+}$ , and is again approximately three times larger than the universal point for  $\pi^-$  production at  $x = -0.5$ . The excess asymptotic value for  $\pi^+$  production vs  $\pi^-$  production at  $x = \pm 0.5$  is presumably due to the net charge = +2 of the overall system and to the fact that these  $x$  regions are not isolated from the quantum numbers of the beam and target at 100 GeV. At  $x = \pm 0.5$  the structure functions with  $A\bar{C}B$  exotic ( $pp \rightarrow \pi^-$ ,  $\pi^+p \rightarrow \pi^-$ ) scale from below, while the structure functions with  $A\bar{C}B$  nonexotic ( $\pi^+p \rightarrow \pi^+$ ,  $\pi^-p \rightarrow \pi^-$ ) scale from above. At  $x = 0$  the structure functions with  $A\bar{C}B$  exotic show a rapid energy dependence scaling from below, while the structure functions with  $A\bar{C}B$  nonexotic show a less rapid energy dependence.

#### ACKNOWLEDGMENTS

We thank the many members of the staff of Fermilab, of the wide-gap-spark-chamber consortium, and of the proportional-hybrid-system consortium for help with the operation of the beam, spark chamber, and bubble chamber. We are grateful to our scanning and measuring staff for their careful work.

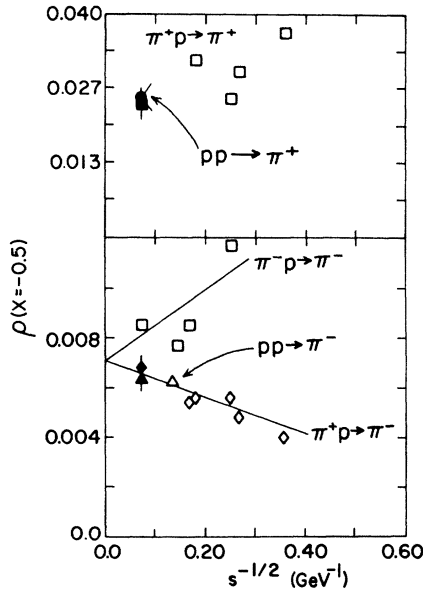


FIG. 11.  $\rho(x)|_{x=-0.5}$  [see Eq. (22)] as a function of  $s^{-1/2}$  for five different inclusive reactions. Lines are drawn to guide the eye. The square boxes are  $\pi^+p \rightarrow \pi^+$ , circles are  $pp \rightarrow \pi^+$ , diamonds are  $\pi^+p \rightarrow \pi^-$ , and triangles are  $pp \rightarrow \pi^-$ . Data of this experiment are the solid symbols.

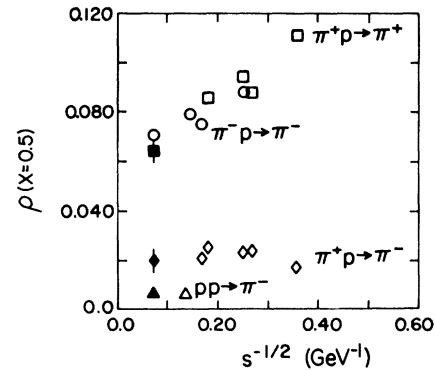


FIG. 12.  $\rho(x)|_{x=0.5}$  [see Eq. (22)] as a function of  $s^{-1/2}$  for four different inclusive reactions. The square boxes are  $\pi^+p \rightarrow \pi^+$ , circles are  $\pi^-p \rightarrow \pi^-$ , diamonds are  $\pi^+p \rightarrow \pi^-$ , and triangles are  $pp \rightarrow \pi^-$ . Data of this experiment are the solid symbols.

\*Work performed under the auspices of the U. S. Energy Research and Development Administration.

- <sup>1</sup>V. E. Barnes, D. D. Carmony, R. S. Christian, A. F. Garfinkel, W. M. Morse, T. A. Mulera, L. K. Rangan, R. N. Diamond, A. R. Erwin, E. H. Harvey, R. J. Loveless, M. A. Thompson, and D. R. Winn, *Phys. Rev. Lett.* **34**, 415 (1975).
- <sup>2</sup>W. M. Morse, Ph.D. thesis, Purdue Univ. (unpublished).
- <sup>3</sup>These events were measured on the Purdue Scanning and Measuring Projector (SMP) system with on-line TVGP geometrical reconstruction with a median rms point scatter on film of about  $7 \mu$ .
- <sup>4</sup>Tracks with bubble-chamber-measured lab momentum above 15 GeV/c, from events which triggered the spark chambers, were extrapolated downstream to the optical spark chambers and an attempt was made to "hook" them to measured sparks in the spark chambers. About 75% of such tracks achieve an acceptable fit, with consequent greatly improved momentum resolution as seen in Fig. 1(b). The failures are due to tracks interacting in the bubble-chamber liquid and walls and to spark inefficiencies in the spark chambers.
- <sup>5</sup>A. S. Carroll *et al.*, *Phys. Rev. Lett.* **33**, 928 (1974).
- <sup>6</sup>W. M. Morse, V. E. Barnes, D. D. Carmony, R. S. Christian, A. F. Garfinkel, L. K. Rangan, A. R. Erwin, E. H. Harvey, R. J. Loveless, and M. A. Thompson, Purdue Univ. Report No. PU-76-438 (unpublished).
- <sup>7</sup>D. S. Ayres *et al.*, *Phys. Rev. Lett.* **35**, 1195 (1975).
- <sup>8</sup>J. Erwin, J. H. Klems, W. Ko, R. L. Lander, D. E. Pellett, P. M. Yager, and M. Alston-Garnjost, *Phys. Rev. Lett.* **32**, 254 (1974).
- <sup>9</sup>C. Bromberg, D. Chaney, D. Cohen, T. Ferbel, P. Slattery, D. Underwood, J. W. Chapman, J. W. Cooper, N. Green, B. P. Roe, A. A. Seidl, and J. C. Vander Velde, *Phys. Rev. Lett.* **31**, 1563 (1973).
- <sup>10</sup>Z. Koba, H. Nielsen, and P. Olesen, *Nucl. Phys.* **B40**, 317 (1972).
- <sup>11</sup>P. Slattery, *Phys. Rev. D* **7**, 2073 (1973).
- <sup>12</sup>J. Whitmore, *Phys. Rep.* **10C**, 275 (1974).
- <sup>13</sup>W. Frazer, L. Ingber, C. Mehta, C. Poon, D. Silverman, K. Stowe, P. Ting, and H. Yesian, *Rev. Mod. Phys.* **44**, 290 (1972).
- <sup>14</sup>J. Lach and E. Malamud, *Phys. Lett.* **44B**, 474 (1973), and references therein.
- <sup>15</sup>The beam (target) diffractive excitation cross sections were obtained by estimating the area above a hand-drawn background of the peak at Feynman  $x \approx -1$  ( $x \approx 1$ ). Details are given in Ref. 6. The double-diffractive excitation cross section ( $\sigma_{DD}$ ) assuming Pomeron factorization is expected to be small compared to the single-diffractive excitation cross section ( $\sigma_{SD}$ ).
- <sup>16</sup>A. R. Erwin, E. H. Harvey, R. J. Loveless, M. A. Thompson, D. R. Winn, V. E. Barnes, D. D. Carmony, R. S. Christian, A. F. Garfinkel, W. M. Morse, and L. K. Rangan, *Phys. Rev. Lett.* **36**, 636 (1976).
- <sup>17</sup>J. Erwin, W. Ko, R. L. Lander, D. E. Pellett, P. M. Yager, and M. Alston-Garnjost, *Phys. Rev. Lett.* **33**, 1352 (1974).
- <sup>18</sup>R. Feynman, *Phys. Rev. Lett.* **23**, 1415 (1969).
- <sup>19</sup>J. Benecke, T. T. Chou, C. N. Yang, and E. Yen, *Phys. Rev.* **188**, 2159 (1969).
- <sup>20</sup>W. H. Sims, J. Hanlon, E. O. Salant, R. S. Panvini, R. R. Kinsey, T. W. Morris, and L. von Lindern, *Nucl. Phys.* **B41**, 317 (1972).
- <sup>21</sup>J. Beauprê *et al.*, *Phys. Lett.* **37B**, 432 (1971).
- <sup>22</sup>T. Ferbel, *Phys. Rev. Lett.* **29**, 448 (1972).
- <sup>23</sup>It has been assumed that in the central region  $\sigma(K^+) = \sigma(K^-) = \sigma(K_S^0)$ . The values obtained from our  $V^0$  data to be published are  $\rho_{\pi^+\pi^0}^{K_S^0}(y^*=0) = 0.053 \pm 0.005$  and  $\rho_{pp}^{K_S^0}(y^*=0) = 0.035 \pm 0.003$ . The proton correction has been made by extrapolating from the region where protons are identified by ionization to  $y^*=0$ . We find  $\rho_{\pi^+\pi^0}^p(y^*=0) = 0.04 \pm 0.01$  and  $\rho_{pp}^p(y^*=0) = 0.09 \pm 0.01$ . Our ratio
- $$\frac{\rho_{pp}^p(y^*=0)}{\rho_{\pi^+\pi^0}^p(y^*=0)}$$
- lies between that found by J. Allaby *et al.* [in *Proceedings of the Fourth International Conference on High Energy Collisions, Oxford, 1972*, edited by J. R. Smith (Rutherford High Energy Laboratory, Chilton, Didcot, Berkshire, England, 1972), Vol. 2, p. 85] at 24 GeV/c and that found by M. Albrow *et al.* [*Phys. Lett.* **40B**, 136 (1972)] at  $s = 2820 \text{ GeV}^2$ .
- <sup>24</sup>C. Bromberg, T. Ferbel, P. Slattery, A. A. Seidl, and J. C. Vander Velde, *Nucl. Phys.* **B107**, 82 (1976).
- <sup>25</sup>W. Morris *et al.*, *Phys. Lett.* **56B**, 395 (1975).
- <sup>26</sup>M. Alston-Garnjost *et al.*, *Phys. Lett.* **39B**, 402 (1972).
- <sup>27</sup>W. Shephard, J. T. Powers, N. N. Biswas, N. M. Cason, V. P. Kenney, R. R. Riley, D. W. Thomas, J. W. Elbert, and A. R. Erwin, *Phys. Rev. Lett.* **27**, 1164 (1971).
- <sup>28</sup>We have also plotted the same data vs  $s^{-1/4}$  (not shown) and within the error bars the data are again consistent with linear scaling. Thus much-higher-energy experiments and/or much smaller systematic uncertainties between different energies are needed to test the validity of the detailed Mueller-scaling forms.